Investigation of the formation of corrugation-induced rail squats based on extensive field monitoring

Deng, Xiangyun; Qian, Zhiwei; Li, Zili; Dollevoet, Rolf

Important note
To cite this publication, please use the final published version (if applicable).
Please check the document version above.

Investigation of the formation of corrugation-induced rail squats based on extensive field monitoring

Xiangyun Deng, Zhiwei Qian, Zili Li*, Rolf Dollevoet

Section of Railway Engineering, Faculty of Civil Engineering and Geosciences, Delft University of Technology, Stevinweg 1, 2628 CN Delft, The Netherlands

ABSTRACT

Rail squats originate from a number of sources, such as corrugations, indentations and welds. A five-year continual field monitoring study was performed on squats induced by corrugations. This study indicated that a small black depression formed at the corrugation under wheel-rail dynamic forces, and then, a primary crack typically initiated on the gauge side edge of the depression. Subsequently, the crack began to propagate in the rail surface in a U shape toward the gauge side in both the traffic direction and the opposite-traffic direction and into the rail toward the field side at an angle of approximately 20°. Rail inclination could influence the crack initiation location and propagation path. The geometry of the black squat depression was initially elliptical, and then, its edge followed the U-shaped cracking path as it grew. The squats turned into a kidney-like shape, typically with a U-shaped crack. Tensile stress likely led to the squat crack initiation and propagation. This cracking phenomenon and mechanism are analogous to the ring/cone crack formation of brittle materials under sphere-sliding contact. As the squats grew further, a ridge formed in the middle part of the depression, and an I-shaped crack appeared at this ridge due to the impact of the wheels. This process eventually led to two-lung-shaped mature squats, typically with a Y-shaped crack. The findings of this paper provide insight into the formation of rail squats.

1. Introduction

Rail squats are one of the main types of rolling contact fatigue (RCF) defects [1]. Squats were reported as black spots dating back to the early 1960s [2]. They are typically observed in the crown of the railhead in straight tracks. A typical mature squat is characterized by a localized, dark depression in a two-lung-like shape, with cracks in the rail surface and under the surface [3,4] (Fig. 1). Further development of cracks leads to rail breakage and thus threatens the safety of rail traffic. In Europe, squats are currently the most considerable RCF threat to rails, and they increase the cost of rail maintenance dramatically. A good understanding of the root causes and formation mechanism of squats contributes to the prevention of such defects from their undesired consequences and to the reduction of the cost of maintenance.

Several comprehensive studies of rail squats have been performed over the past few decades. Clayton and Allery [1] conducted a pioneering metallurgical analysis of mature squats and found that cracks initiate due to shear stresses and propagate into the rail. The development of these cracks coincides with the formation of black spots in the rail running surface. Pal et al. [5,6] also performed some metallurgical observations and pointed out that the crack initiation in the rail surface was related to microstructural changes and the consequential white

etching layer (WEL) and ratcheting. Grassie et al. [7] argued that the WEL is not a necessary condition for squat initiation, and squat-like defects associated with the WEL could be classified as studs. Simon et al. [8] presented a tribological characterization of squats, considering plastic deformation, surface microstructures and crack fronts. Bogdanski et al. [9,10] investigated the fracture phenomenon and liquid entrapment mechanism for squat cracks by calculating stress intensity factors using linear elastic fracture mechanics. Farjoo et al. [11] conducted a similar study, further considering the resulting bending effects of the elastic foundation on crack propagation through stress intensity factors. Steenbergen et al. [12] studied squat formation, in which RCF produced a leading crack and developed via trailing brittle failure cracks into the squats. These works concerned mature squats with large cracks. Satisfactory mechanisms of squat crack initiation and development were still missing.

Li et al. [3,4,13,14] conducted a series of investigations on squat initiation and growth. In these investigations, the initiation sources were classified into two types of rail surface irregularities, i.e., the active type and the passive type. The active type includes short pitch corrugation and rail welds. The common characteristic of this type is that the irregularities and the resulting squats arise internally and spontaneously from the consequence of imperfect design, construction
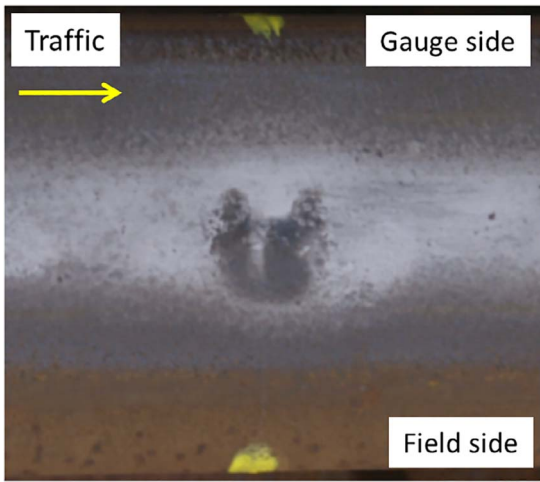
Fig. 1. A typical squat in a two-lung shape with cracks at the monitored site.

or maintenance of tracks. The irregularities at corrugation are resulted from dynamic forces excited by corrugation, and the irregularities at welds are developed from differential wear and differential plastic deformation because of material inhomogeneity. This type of irregularities initiate and grow by themselves. The passive type includes indentations and wheel burns, the latter is also called rail burns in [13]. In contrast to the active type, the passive type are generated by external objects such as bearing rollers/balls and spinning wheels (wheel slip) [4]. In addition to the afore-mentioned active and passive types, further observations have shown a third type of initiation sources, i.e., irregularities by design, such as insulation joints [15] and crossings [16];

both the gaps at the joint and the crossing cause battering of the rail by passing wheels, thus squats.

In spite of the three types of very distinctive initiation sources, mature squats bear a typical common appearance of two-lung shape with typical U (or V) and Y shaped cracks [4]. Numerical analysis and filed observations [3,4] showed that this two-lung shape is the result of the dynamic wheel-rail contact force induced by the irregularities. It was also found that the irregularities and their resulting squats can induce corrugation-like wave patterns. These patterns occurred immediately after squats. Both the appearance and wavelengths of them are similar to those of short pitch corrugation in the Dutch railway network. A numerical approach for determining the critical size for squats to initiate from the passive type irregularities was presented in [13]. The above numerical works [3,4,13,14] assumed that cracks were not deep enough to significantly affect the relevant wavelengths, therefore, cracks were not considered in the models. Li et al. were mainly interested in the primary and root causes of the two-lung shape of squats when cracks are in their initiation and early stages of growth, the assumption that cracks were not deep is therefore reasonable.

A clear distinction was made between the corrugation-induced squats and the squat-induced corrugation-like wave patterns in [4]. In principle, all the afore-mentioned initiation sources but the corrugations could cause squat-induced corrugation-like wave patterns. A field survey reported in [4] showed that among all the squats 33% were caused by corrugation; among the other 67% of the squats, 61% had wave pattern following them, and the other 39% not. Some authors call the squat-induced corrugation-like wave patterns also corrugation [17].

By considering dynamic effects, recently, Andersson et al. [18] investigated the propensity of squat initiation by examining the effects of surface irregularities on local stresses using two-dimensional (2D)
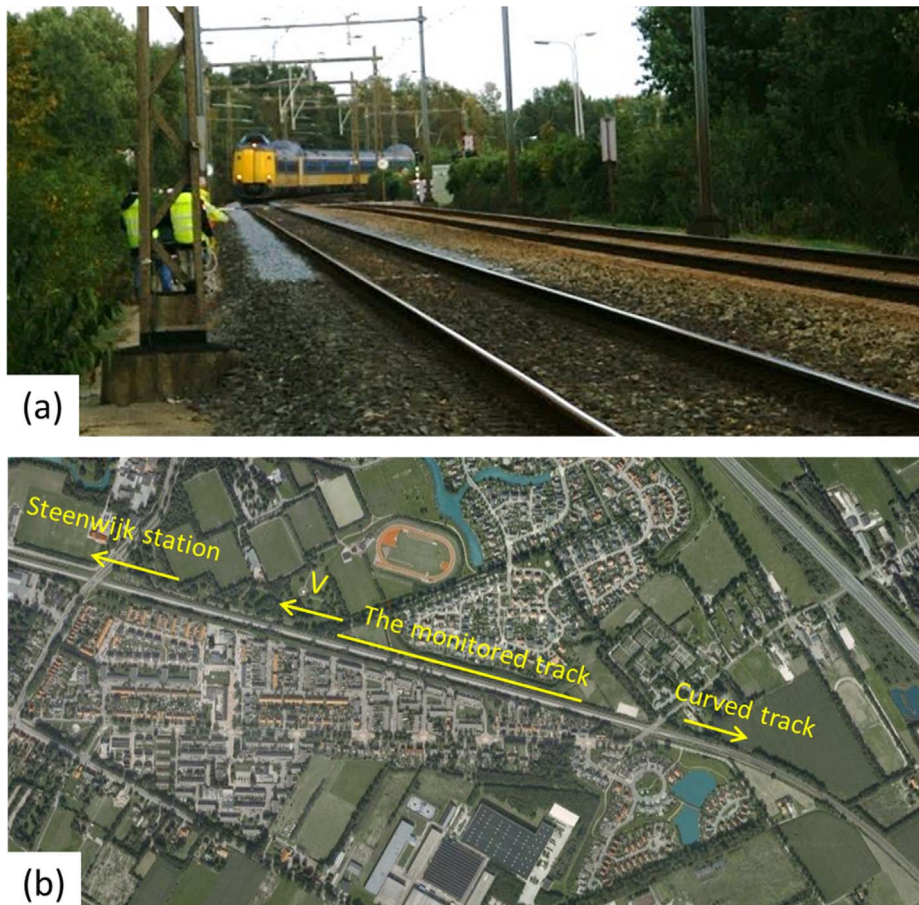

Fig. 2. Overview of the monitored straight track: (a) Monitored track looking in the direction of the curve against the traffic; (b) Google satellite view of the site.

numerical models. Experimental study or field observation was not presented in this work. Crack growth and geometry evolution of squats were also not included.

Cracks, however, are the most dangerous aspect of squats. As corrugation-induced squats consist a major part of the squats population, and the initiation and early growth of the cracks have not yet been investigated. Therefore, the present work focuses on this type of squats. The objective is to reveal the formation of corrugation-induced squats and the accompanying crack initiation and propagation processes based on the observations and analyses of a five-year continual field monitoring. The focus is on primary virgin cracks, in other words, the origins of the squats and the accompanying cracks were not residual cracks of previous damages. This study contributes to a better understanding of the root causes of rail squats and RCF-related phenomena.

2. Description of the field monitoring

A straight section of the Dutch railway network was selected for a five-year continual field monitoring of squat initiation and evolution. The monitored track was located in Steenwijk in the Netherlands, as shown in Fig. 2. During the period from 2007 to 2012, ten field observations were conducted at intervals of approximately 6 months. Two times of grinding were performed on the monitored track during the period of the monitoring. The first one was performed between the fifth monitoring observation (November 2009) and the sixth observation (June 2010) with a material removal of 1.1 mm (including natural wear by traffic because these 1.1 mm were derived from the profiles measured during the fifth and sixth observations); the second one was performed between the seventh observation (April 2010) and the eighth observation (August 2010) with a material removal of 0.3 mm (including natural wear). There was no grinding before the start of the monitoring. One-directional traffic ran on the track at a frequency of approximately 20 min per train during the day and no trains during the night. The majority of the traffic consisted of passenger trains. The maximum axle load of the trains was approximately 22 tons [19], and the annual traffic load was about 3.4 MGT. When trains were running on the straight section, they had just exited a curved track. The speed of the trains was 130 km/h and some traction was needed to maintain this speed. The rails were of the R260Mn grade with UIC54E1 as the nominal profile with a weight of 54 kg/m. They were installed in the track in 1989.

The section of track was selected for monitoring because of the following reasons. First, some corrugation and resulting squats of various severities were observed at the beginning of the monitoring, as shown in Fig. 3(a). In view of the active nature of corrugation-induced squats, it was predictable where new squats would initiate and grow from the developing corrugation. This makes a fruitful selection of monitoring locations possible. The second reason is that there were no visible defects or residual cracks in the rail surface other than the intended corrugation and squats. The third reason is that the rails had not been ground. To prove that any grinding was not performed before the start of the monitoring, the rail profiles measured during the monitoring at a number of defect-free locations were analyzed. It was found that the average rail head loss due to the natural wear was 0.07 mm/year between the first and fifth observations, and the average rail head height loss was 0.06 mm/year between 1989 and 2007. The height loss of 0.06 mm/year would have not been possible if any corrective grinding had taken place. This was further confirmed by looking at the measured profiles, as shown in Fig. 3(c) and (d), where the measured profiles are aligned with the nominal profile (in black) on the field side (the left side). The measurements show good repeatability. The profile (in magenta) measured immediately after a corrective grinding at the sixth observation is as smooth as the other profiles on the gauge side. In contrast, the ground profile has a larger rail head height loss (see Fig. 3(d)) and a sharp turning point at the field side (indicated in Fig. 3(c)), apparently it is different from other profiles. If there was any

earlier grinding, such a larger height loss and sharp turning point should be recognizable in the first measurement.

During the monitoring, more than 100 squats of various severities were observed. These squats initiated and developed from short pitch corrugations because they occurred in the middle of the corrugation [4]. Several examples of squats at the first and fifth observations are shown in Fig. 3(a) and (b). Among the ten field observations, the first five observations were performed before the first rail grinding. Dozens of selected squats were photographed during each observation. The cross-sectional profile and vertical-longitudinal profile at the squats were measured using the MiniProf and RailProf devices, respectively. Non-destructive tests were conducted to detect cracks under the rail surface. These tests included eddy current tests using an Elotest D 300, which can capture shallow cracks under the rail surface, and ultrasonic tests using a Krautkramer USM 25, which is able to detect deeper cracks [4].

By the fifth observation (shortly before the rail grinding), 30 squats were mainly traced. Among them, 9 squats were light, 17 were moderate, and 4 were severe. The analysis in this paper is mainly based on these 30 squats, with consideration of supporting evidence from the remaining squats and from several of the other monitoring observations at this monitored site. Eleven of the 30 squats are shown in Figs. 1, 3–7, 9, 10, 14, 15 and 17 to provide as much direct information as possible.

3. Field observations and analysis

The initiation and evolution processes of the squats are postulated based on a continual field monitoring and analysis. The following aspects are considered in this investigation: the geometry of the squats (size and shape) and the accompanying cracking phenomena. A squat development process is proposed based on the observations and analyses.

3.1. Squat initiation and cracking processes observed over time

3.1.1. Critical crack initiation size and point in the lateral direction and U-shaped cracks

The series of photographs in Fig. 4, which were obtained during the first six field observations, show the evolution of a squat. The changes in size and in the bright running band near the squat can be seen. At the time of the first observation, the squat was a small black depression in an approximately elliptical shape with a size of approximately 5 mm in the lateral direction and 6 mm in the traffic direction. The position of T1 is approximately 4 mm from the rail centerline. This black depression did not have visible surface cracks. It was growing in size until the fifth observation, shortly before the rail grinding. The squat eventually evolved into a kidney-like shape with its concave part resembling a shallow U, as seen in Fig. 4(d) and (e). As will be shown later, this shallow U developed into a full U that was the primary surface crack of the squats. Thus, this concave part is referred to hereafter as U-shaped. At the time of the fifth observation, the running band at the squat was widened on the gauge side, as indicated by the shining part above point T1, indicating that the depression broadened the running band.

Although it was hard to confirm the presence of surface macrocracks by visual inspection during the first five observations, eddy current tests showed that a crack began to appear as of the second observation. At this time, T1 of the depression was approximately 6 mm from the rail centerline, and the dimension of the depression was approximately 8 mm in the lateral direction and 9.5 mm in the traffic direction. These results indicate that cracks initiated when the black depression grew to a certain size. This finding was confirmed by the observations of another 5 squats of the 30 selected squats, which did not have macrocracks in the beginning, but cracks were observed at the sixth observation. This finding is in line with the critical size of squat initiation that was numerically derived in [13] by comparing the maximal von Mises stress with tensile strength, and the material was also R260Mn.
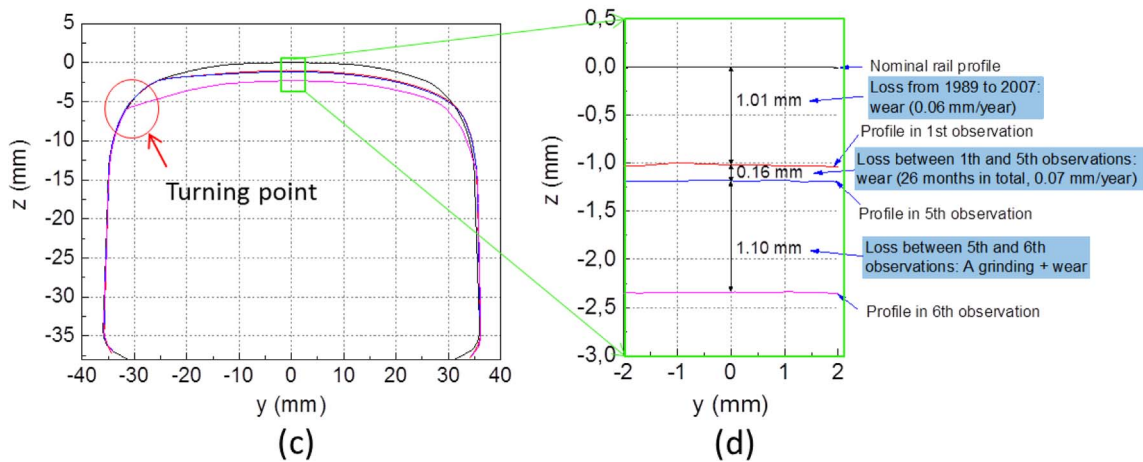
Fig. 3. Typical corrugation with several squats of various severities adjacent to a monitored squat and measured rail profiles for analysis of grinding: (a) in the first observation, corrugation and some squats already existed adjacent to a monitored squat; (b) in the fifth observation, the corrugation and squats in (a) had become severe and new squats of different severity appeared; (c) measured rail profiles by MiniProf in the vicinity of one squat: from top to down they were the nominal (black) and those measured in the first (red), fifth (blue) and sixth (magenta) observations, respectively; (d) zoom-in of (c) in the middle of the profiles. (For interpretation of the references to color in this figure legend, the reader is referred to the web version of this article.)

After the crack had appeared, the shape of the depression began to change into a kidney-like shape, and the location of T1 remained approximately 6 mm from the rail centerline. Eddy current tests and ultrasonic tests showed that the crack continued to grow after their initiation. The phenomenon of crack growth with the fixed location of T1 relative to the rail center was observed with all the other monitored squats.

After the rail grinding to a depth of 1.1 mm, the black depression was removed, and a shallow U-shaped crack was exposed, as shown in Fig. 4(f). This observation shows that the crack had propagated into the rail deeper than 1.1 mm and that the depth of the black depression was less than 1.1 mm. This finding confirmed the presence of the cracks measured by the eddy current tests and ultrasonic tests. The removal of the black depression and the exposure of the residual cracks were also observed at the other monitored squats with cracks deeper than

1.1 mm.

3.1.2. U-shaped crack initiation position in the rolling direction over the complete squat development process

Fig. 5 illustrates the development process with another squat. The figure consists of six photographs from the first five consecutive observations before the rail grinding and from the seventh observation after the grinding; the photo from the sixth observation was not sufficiently clear. These photographs show that T1 was the bottom point of the U shape and that its position stayed fixed not only in the lateral direction, as demonstrated with Fig. 4, but also in the traffic direction. The latter concluded as follows: the rail head has a constant width of 72.2 mm. With this value, the sizes of the depressions and cracks were derived from the photos for this paper. In Fig. 5, there is, beside the squat, another small black spot. With the known rail head width, the
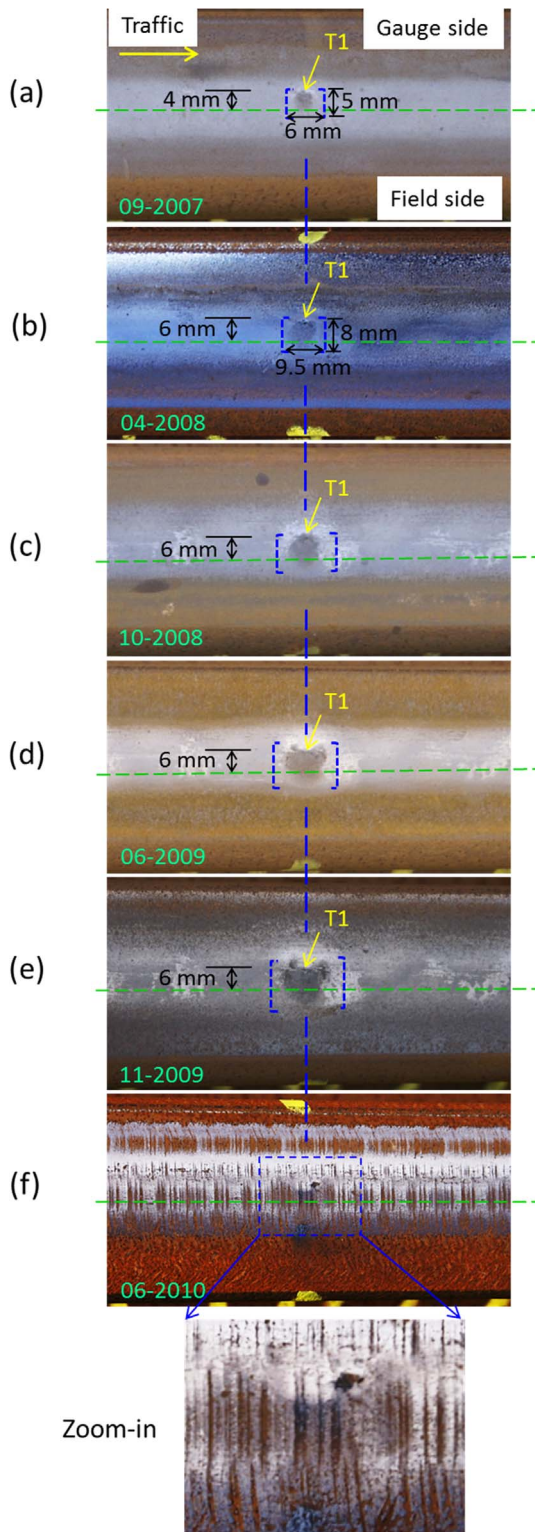
Fig. 4. Evolution of a squat with the critical size of 8 mm for crack initiation and subsequent cracking (the dashed straight green line represents the rail centerline): (a)–(e) Before rail grinding to a depth of 1.1 mm; (f) after the rail grinding, revealing a shallow U-shaped crack, as seen in the zoom-in. (For interpretation of the references to color in this figure legend, the reader is referred to the web version of this article.)
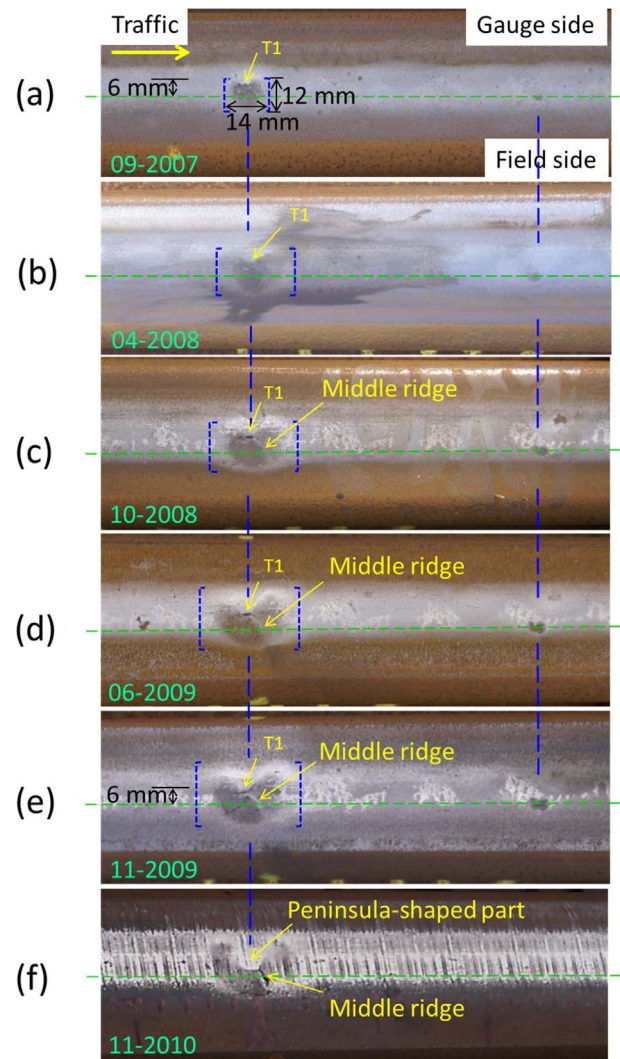

Fig. 5. Confirmation of the crack initiation point according to the relative positions of the black spot and point T1 (the green line represents the rail centerline): (a)–(e) Before rail grinding; (f) after rail grinding to a depth of 1.1 mm. (For interpretation of the references to color in this figure legend, the reader is referred to the web version of this article.)

distance between the small black spot and point T1 is determined, and it can be seen in Fig. 5 that T1 remained at a constant distance from the small black spot.

With T1 aligned according to the blue dashed lines, Fig. 5 shows that the squat grew longitudinally in both the traffic and opposite-

traffic directions as well as laterally toward the gauge side and field side simultaneously. This growth pattern was observed at all 21 of the moderate and severe squats. The squat in Fig. 5 first grew into a kidney-like shape with the concave part of the kidney bounded by a U-shaped crack, and then it gradually evolved into a two-lung shape with a middle ridge (Fig. 5(c)–(f)). After the grinding, the part bounded by the full U-shaped crack took on a peninsula-like shape, as seen in Fig. 5(f). A more detailed discussion about the formation of the middle ridge and the peninsula-shaped part is in Sections 3.4.1 and 3.4.2. Notably, the typical two-lung shape and the peninsula-like shape were not clearly observable at the squat in Fig. 4 because the squat was still in a relatively early stage; the crack and geometry had not yet grown into the typical shape.

The very small black spot in Fig. 5(a), barely visible to the naked eye, was growing before the grinding. At the fifth observation, it turned into an obvious surface depression; its size was already comparable to that of Fig. 4(a), and it should have been able to develop into a squat if not removed. The initiation and growth of black spots are, in the very beginning, driven by the corrugation. At the same time, the black spots are rail surface irregularities that excite (additional) dynamic contact force; the larger the black spot, the larger the dynamic force, creating a positive feedback loop that promotes the continuous and accelerates
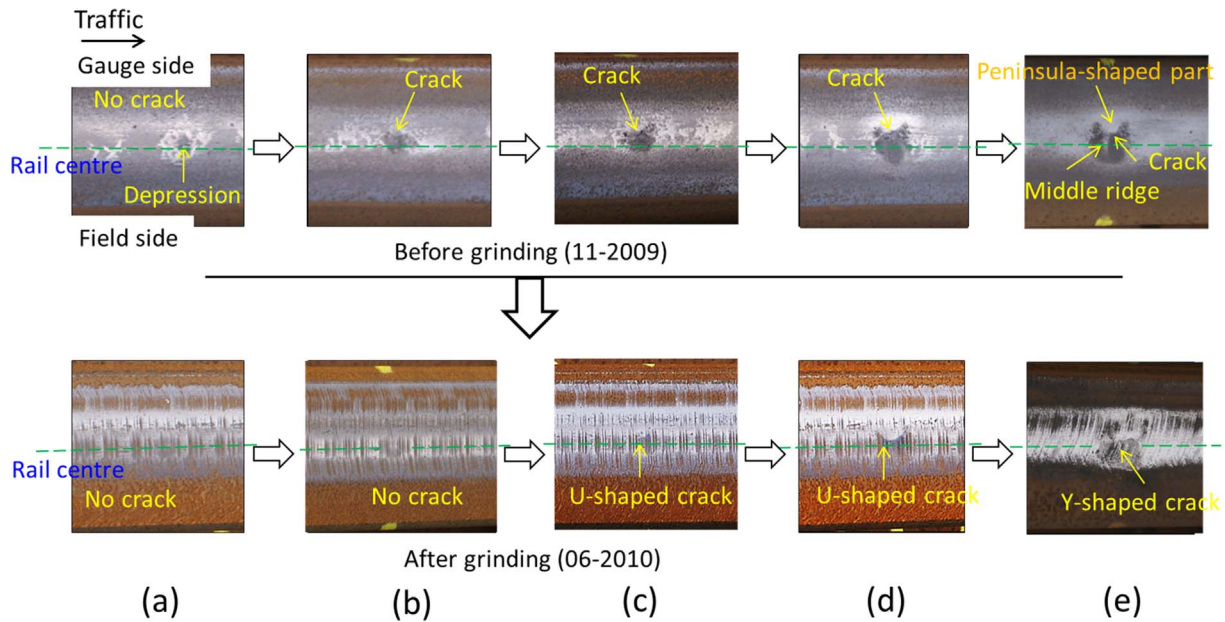
Fig. 6. Different squats at various severities: earlier stages to later stages.

growth of the black spots into squats. Combining these observations, a complete picture is obtained of how a mature squat is developed from the smallest visible black spot. The longitudinal position of the crack initiation point should be close to the location of the very first visible black spot.

3.2. Surface and subsurface cracks at squats of different severities

To further show the growth process of the squats from early stages to mature stages, five squats of different severities are presented in Fig. 6. The top five photographs were obtained at the fifth observation before the rail grinding, and the bottom five were obtained at the sixth observation after the grinding. The photographs are shown from left to right with increasing severity; therefore, they can be interpreted as a representation of five different steps in a squat over its life cycle.

In (a), the black depression was still significantly smaller than the critical size of 8 mm; no crack was observed in the rail surface either before or after the rail grinding, as seen in Fig. 6(a). It is reasonable to assume that the macrocrack had not yet initiated at this time. In (b), the size of the depression (10 mm (in the lateral direction) × 14 mm (in the traffic direction)) was larger than the critical size of crack initiation; a small surface primary crack became visible at this stage prior to the rail

grinding (see the arrow in Fig. 6(b)). After the grinding, the crack was removed. This observation suggested that the crack was shallower than 1.1 mm. In (c) and (d), the squats were in a kidney-like shape before the grinding, and a U-shaped crack became visible after the grinding. The length of the U-shaped crack continued to grow from the bottom along the U in both directions, i.e., in the traffic and the opposite-traffic directions, with the evolution of the squat. These observations confirm that the bottom of the U-shaped cracks was the initiation point of the cracks in or near the rail surface on the gauge side of the depression. The point of the crack initiation corresponded to position T1 in Figs. 4 and 5. After initiation, the crack propagated along the U shape, as well as into the rail toward the field side, as discussed in Sections 3.3 and 3.4. Moreover, the crack grew more rapidly in the traffic direction than in the opposite-traffic direction; see the discussion in Section 4.3. In (e), the squats reached a more severe stage: they evolved into the two-lung shape with a middle ridge, and an I-shaped crack appeared at this ridge after the grinding. More details about the I-shaped crack are provided in Section 3.4.

From the above analysis, it can be concluded that the crack initiation point is in the rail surface or at least in the top layer of material not deeper than 1.1 mm from the surface.

Although the shape of the black depression at the very beginning
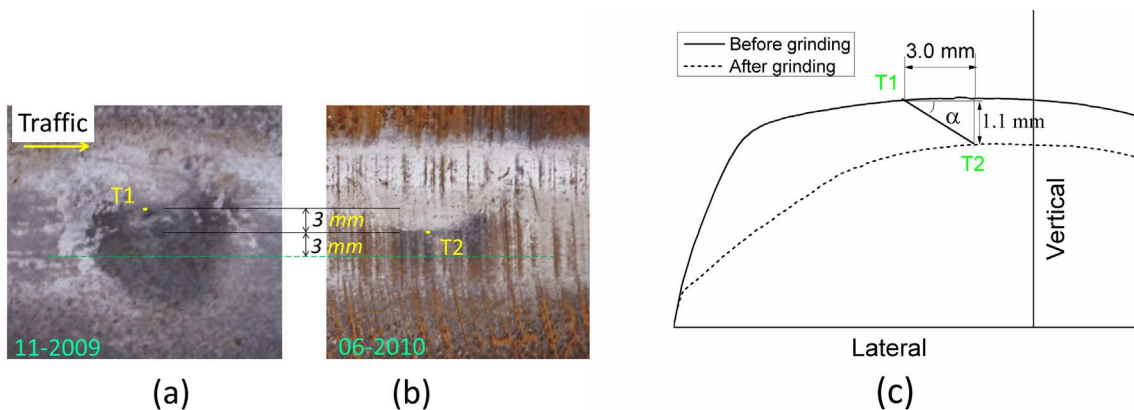
Fig. 7. Determination of the cracking angle relative to the rail surface in the vertical-lateral cross-section (the green line represents the rail centerline; T1 and T2 denote the bottom of the U-shaped crack): (a) Before rail grinding; (b) after rail grinding to a depth of 1.1 mm; (c) cross-sectional profiles of the rail. (For interpretation of the references to color in this figure legend, the reader is referred to the web version of this article.)
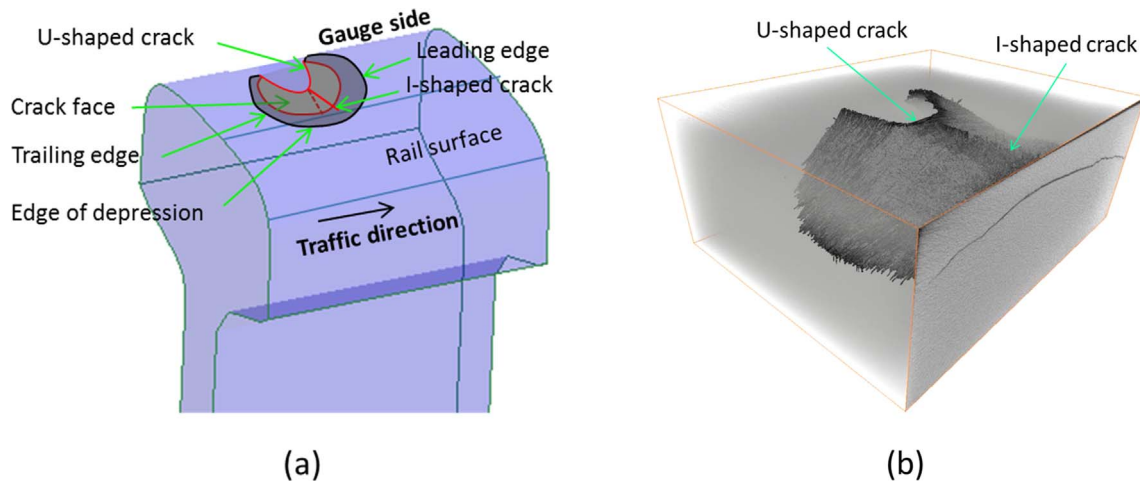
Fig. 8. 3D crack face in a two-lung-shaped squat: (a) Inferred from the surface-visible Y shape and the cracking angle α of Fig. 7(c); (b) obtained from specimen 2b (squat caused by corrugation) from [20] with computed tomography, courtesy of Meysam Naeimi.
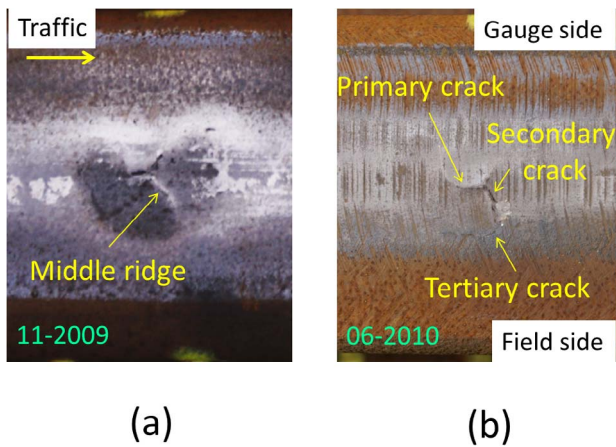

Fig. 9. A typical two-lung-shaped squat with a Y-shaped crack and a semi-circular tertiary crack (the same squat as in Fig. 5): (a) Before rail grinding; (b) after rail grinding to a depth of 1.1 mm.
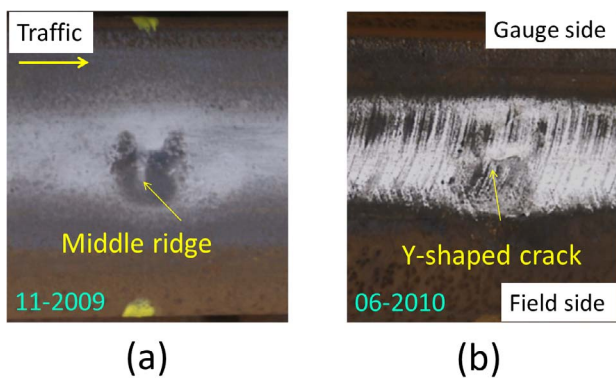

Fig. 10. Another typical two-lung-shaped squat with a Y-shaped crack (the same squat as in Fig. 6(e)): (a) Before rail grinding; (b) after rail grinding to a depth of 1.1 mm.

was not very clearly visible, as shown in Fig. 6(a), the convex part of the kidney-shaped depression was elliptical, as seem in Fig. 6(b)–(d), and this elliptical shape most likely originated from the elliptical contact area between the wheel tread and the rail crown. The elliptical shape is more clearly visible in Fig. 4, especially in Fig. 4(a) and (b). Therefore, the small black depression in (a) should have been approximately elliptical in shape.

3.3. Cracking angle

A moderate squat with a U-shaped surface crack was examined to determine its cracking angle in the vertical-lateral cross-section, which passes through the bottom of the U shape, as shown in Fig. 7. In Fig. 7(a), bottom point T1 of the crack was the crack initiation point, and it was located on the gauge side at a distance of 6 mm from the rail centerline. After the rail grinding to a depth of 1.1 mm, the bottom of U-shaped crack T2 shifted 3 mm toward the field side, as shown in Fig. 7(b). The cracking angle α was then approximately 20°, as illustrated in Fig. 7(c), indicating that the surface crack propagated into the rail at an angle of approximately 20° toward the field side. This finding agrees with the findings in the computed tomography investigation in [20].

For verification purposes, another 18 moderate and severe squats with cracks on the gauge side were also examined. All the crack initiation locations were approximately 6 mm from the rail centerline on the gauge side. These locations were also the bottom points of the U-shaped cracks of the squats, and they corresponded to point T1. After the rail grinding to a depth of 1.1 mm, the bottom points moved 3 mm toward the field side. Thus, the cracking angles were again approximately 20° for all the examined squats, 7 of which are shown in Figs. 1, 4–7 and 15. All the results were in good agreement with the cracking angle shown in Fig. 7.

3.4. Crack shape in 3D and secondary cracks

3.4.1. The primary U-shaped crack in 3D

The U-shaped crack initiated at the bottom point of the U and then propagated toward the gauge side in both the traffic and opposite-traffic directions simultaneously, as illustrated in Fig. 8. The crack also propagated into the rail at an angle of approximately 20°. This cracking process was observed at more than 20 monitored squats, as shown above. Based on this finding, the shape of the crack was constructed and is shown in Fig. 8(a). This shape was verified with 3D computed tomography [20], as seen in Fig. 8(b).

In Fig. 8, the crack face encloses a peninsula-shaped part. The intersection of the peninsula-shaped part with the rail surface is a U-shaped crack. When the U-shaped crack grows, the two arms of the U extend toward the gauge side; this makes the peninsula-shaped part longer. At the same time, the crack propagates downward into the rail, i.e., the peninsula-shaped part extends deeper into the rail. Consequently, the depressed area grows with the peninsula-shaped part simultaneously in both the surface dimension and depth.

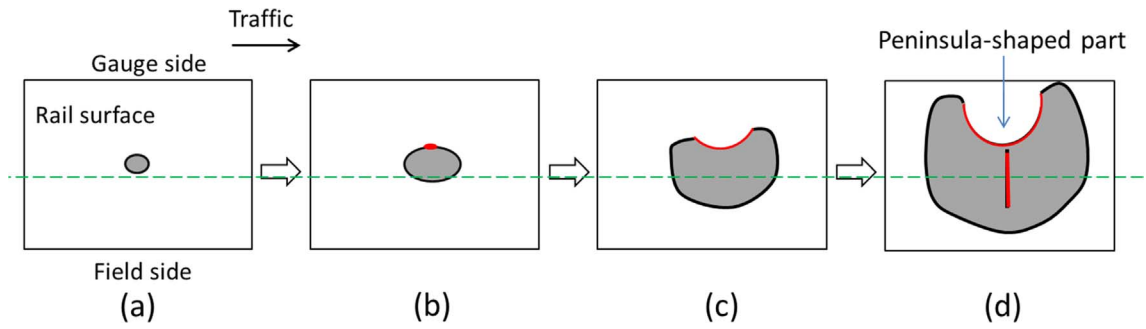Thus this peninsula-shaped part increasingly becomes an obstacle to

Fig. 11. Schematic diagram of the squat development process, including crack initiation and growth. The green line represents the rail centerline, the red line represents the cracks, and the gray area represents the squat/black depression with the black curved line representing its edge: (a) Elliptical small black depression; (b) crack initiation point, usually on the gauge side edge of the black depression; (c) U crack starts to form, causing the elliptical depression to become kidney shaped; crack propagates slightly more rapidly in the traffic direction due to traction force; (d) two-lung-shaped mature squat with a Y-shaped crack. (For interpretation of the references to color in this figure legend, the reader is referred to the web version of this article.)

the rolling wheels, and impact occurs when the wheels meet the peninsula-shaped part and fall from the peninsula-shaped part. These two impacts are clearly seen from the two shining patches at the peninsula-shaped parts and at the leading edges (see Fig. 8 for definitions of leading and trailing edges) of the black depressions in Figs. 1, 3, 4(c)–(e), 5(c)–(e), 6(d)–(e), 7, 9, 15 and 17. The two impacts correspond to peak contact forces B_2 and C_2 in Fig. 8(b) of [3]. Thus, the development process of the squats initiated from the corrugation and converged with the squat growth process postulated in [3] and validated in [4], although the initiation sources are different: in [3], the squats were assumed to be caused by pre-existing rail surface defects, such as indentations and wheel burns; these squats belong to the passive type [13] that are caused by external factors. Corrugation-induced squats belong to the active type because these squats arise spontaneously due to defective tracks.

3.4.2. Secondary I-shaped crack

The two impacts at the peninsula-shaped part punched and pushed the depressed rail material so that a "ridge" was formed in the middle of the black depression, as indicated in Fig. 9(a). This ridge is clearly shown on the surface in Figs. 1, 5(c)–(f), 6(e), 9, 10 and 15. Cracks can develop at the middle ridge, as seen in Figs. 5(f), 6(e) and 8–10, especially in severe squats. This crack is the secondary I-shaped crack. The I-shaped crack is also shown in the 3D geometry of the crack in Fig. 8(b).

3.4.3. Y-shaped crack and the two-lung shape of squats

When the U-shaped crack and I-shaped crack occur simultaneously, they together become a Y-shaped crack, as shown in Figs. 9 and 10. The Y divides the elliptical shape into the shape of two lungs, which occurs with the typical shape of severe squats.
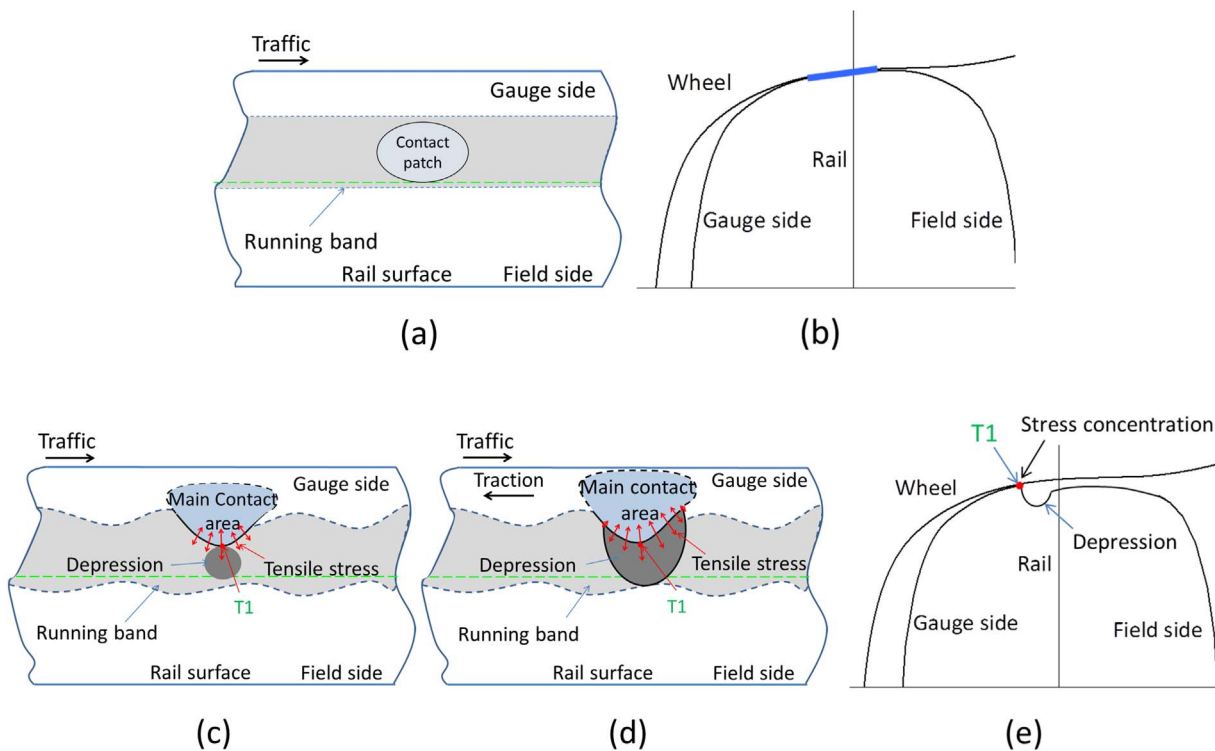
Fig. 12. Wheel-rail contact patch. The green line represents the rail centerline; the blue dashed lines mark the running band and corrugation; and the blue solid line indicates the main contact area: (a) and (b) When the rail is smooth; (c) and (e) when corrugation and a small black depression exist. The red arrows indicate tensile stress along the border of the main contact area; the length of the arrows is schematically proportional to the magnitude of the tensile stress. (c) corresponds to Fig. 11(b), and (d) corresponds to Fig. 11(c) and (d). (For interpretation of the references to color in this figure legend, the reader is referred to the web version of this article.)

Fig. 13. Positions of the main contact areas (indicated by the blue line) that determine the locations of the primary cracks: (a) Rail inclination of 1/40; (b) a slight increase in the rail in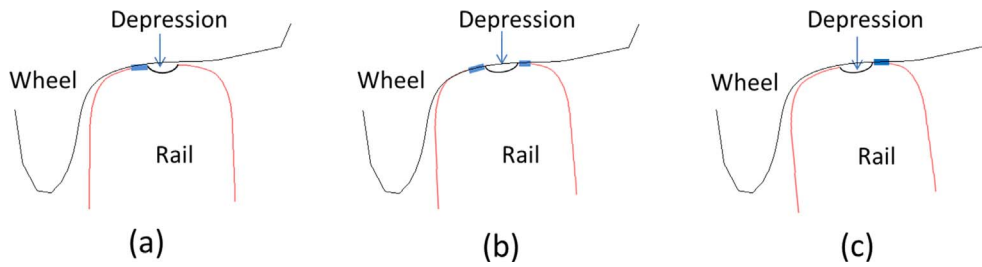clination; (c) a larger increase in the rail inclination. (For interpretation of the references to color in this figure legend, the reader is referred to the web version of this article.)
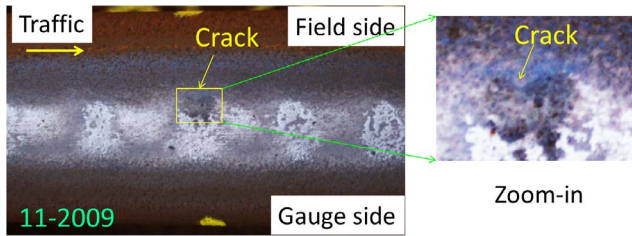

Fig. 14. A squat with a primary crack on the field side edge of the black depression.
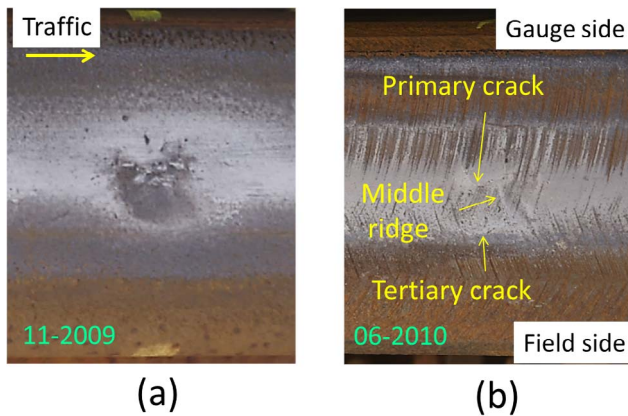

Fig. 15. A squat with two cracks, i.e., a primary crack and a tertiary crack: (a) Before rail grinding; (b) after rail grinding to a depth of 1.1 mm.

Fig. 16. Evolution of the squat geometry. S1 and S2 indicate the two vertical-longitudinal sections.

3.5. Squat development process

Based on the observations and analyses described above, a squat development process is proposed. A schematic diagram of the process is shown in Fig. 11 to describe the squat evolution and cracking processes.
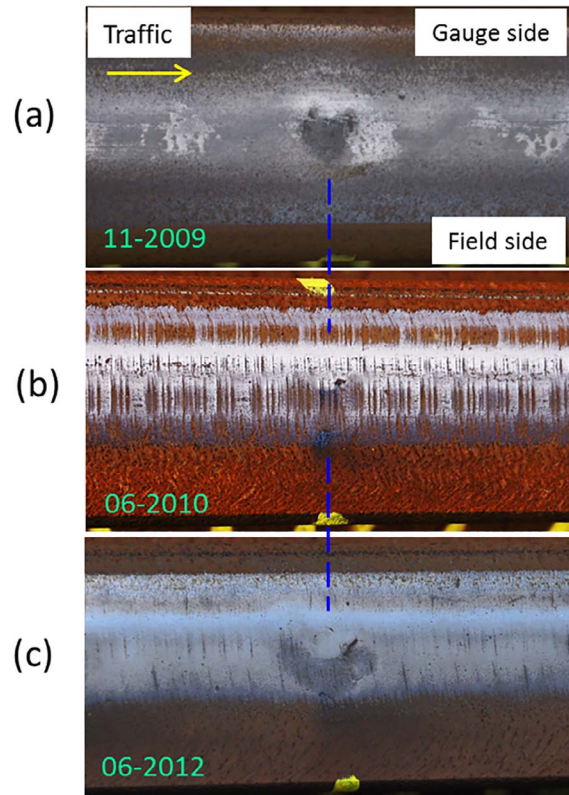

Fig. 17. Squat (the same as in Fig. 4) development after rail grinding: (a) Fifth observation before rail grinding; (b) sixth observation after grinding to a depth of 1.1 mm; (c) tenth observation after another grinding of approximately 0.3 mm between the seventh and eighth observations.
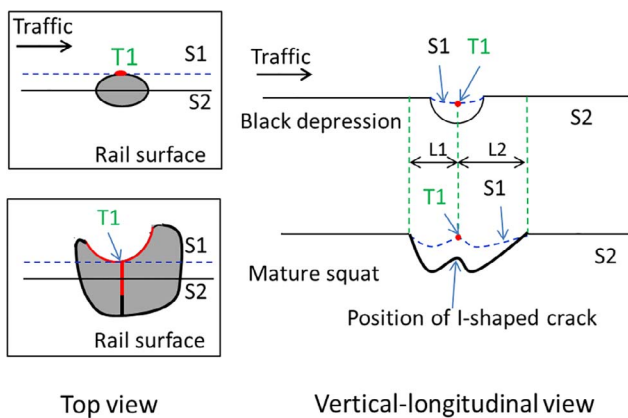
Initially, a small black depression is generated at a corrugation (Fig. 11(a)). The black depression results from microcracks due to plastic deformation and work hardening in the surface layer of the rail material, typically up to a depth of 1.1 mm, and it is caused by the cyclic wheel-rail impact forces excited by the corrugation. The black depression grows roughly in the shape of a complete ellipse until it reaches a critical size, and a primary macrocrack is initiated in/near the rail surface on the gauge side edge of the depression (Fig. 11(b)). Then, the shape of the black depression starts to change and follows the propagation of the crack, while the uncracking part remains elliptical. The surface crack propagates in a U shape toward the gauge side in both the traffic direction and the opposite-traffic direction (Fig. 11(c)). This process forms a U-shaped crack with the bottom point of the U being the initiation point of the primary crack. In this stage, the squat becomes a kidney-like shape with a concave part in the middle region bordered by the U-shaped crack. Moreover, the squat grows more rapidly in the traffic direction if the longitudinal contact force is tractive. It also propagates into the rail toward the field side at an angle of approximately 20°. When the squat grows to a certain stage, a ridge is

formed in the middle of the black depression, and an I-shaped crack can occur at this ridge. The combination of the U-shaped crack and I-shaped crack forms a Y-shaped crack (Fig. 11(d)). In this process, the U-shaped part grows into a peninsula-like shape around the time of the formation of the I-shaped crack. Eventually, this evolution process leads to a mature two-lung-shaped squat with a Y-shaped crack. The proposed development process is derived from and is valid for corrugation-induced squats, and it is elaborated in the next section.

4. Elaboration on the squat development process

The proposed squat development process is discussed in detail in this section. The following aspects are addressed: the formation of the small black depression, the crack initiation and propagation, and the influence of the rail inclination on the initial cracking locations.

4.1. Formation of small black depressions with reduced tensile strength

In the running band, the rails are subjected to large cyclic wheel-rail interaction forces. These forces produce repeated plastic deformation and work hardening associated with microcracks [21]. The plastic deformation and work hardening deteriorate the RCF resistance [22], in turn increasing the brittleness of the materials. As a result, macrocracks initiate more rapidly when new crack initiation mechanism arises. The crack can initiate in the manner of the growth of a single microcrack or the coalescence of many microcracks, as noted in [23] and [24].

When corrugation is present, the plastic deformation and work hardening typically occur most significantly at the places where the dynamic contact stress is greatest. When the hardening reaches a degree of saturation, the ductility of the rail material is exhausted, and the local material becomes brittle accompanied by a network of microcracks. The network of microcracks expands in the rail surface layer and causes the surface to collapse locally to form a small elliptical black depression, such as those shown in Figs. 4–6.

4.2. Crack initiation by mode I fracture

When a small black depression grows to a certain size, it significantly changes the effective contact patch at the wheel-rail interface, as illustrated in Fig. 12. The contact patch can be approximated as elliptical when the rail surface is smooth, as shown in Figs. 12(a) and 10(b). However, its location and shape are different in the region when a small black depression exists. The main contact patch at the depression shifts to the gauge side, as shown in Fig. 12(c) and (d). The border of the main contact area at the edge of the depression exhibits a U shape with the opening of the U facing toward the gauge side. The U shape comes from the intersection of the wheel and the rail surfaces as a wheel is loaded onto a rail. This change in the contact patch is generalized and marked in Fig. 12(c) and (d). This main contact area is most clearly indicated by the brighter contact area bordered by the U-shaped crack at the monitored squats, such as those seen in Figs. 1, 4(d) and (e), 5, 6(d) and (e), 7, 9, 10, 15 and 17.

The region at the black depression sustains the impact from the wheels; the dynamic force is large. At the same time, the depression causes stress concentration at edge T1, as seen in Fig. 12(c), (d) and (e). The large contact force and stress concentration lead to stress that is much larger than elsewhere on the rail surface. According to the Hertz theory [25], tensile stress is present immediately outside the contact patch, and its value is maximal at the border of the contact. In the case of corrugation with surface depression, a tensile stress distribution arises along the border of the main contact area in a U shape, as indicated by the red arrows in Fig. 12(c). The tensile stress is the greatest at T1. Since the material at the depression is brittle, this greatest tensile stress results in a macrocrack at T1 by mode I fracture. This crack initiation phenomenon is analogous to the ring/cone crack formation of brittle materials under sphere contact [26] and the formation of crack

in RCF by asperities [27]. Note, T1 is located on the gauge side edge of the depression approximately 6 mm from the rail center for most of the squats in the present work. It could change depending on the profiles of wheels and rails, the local track conditions and the material property.

4.3. Crack propagation into the U shape

Once this primary crack is present, the tensile stress drives it to propagate along the border (the solid black line in Fig. 12(c) and (d)) of the main contact area in a U shape by stress concentration and mode I fracture toward the gauge side in both directions of the U-shaped crack. This fracture mode was observed in [8]. It forms the U-shaped primary cracks.

When traction force is applied, the additional shear stress adds tension to the leading side of the contact patch and subtracts from the tensile stress on the trailing side [28]. Therefore, the resulting tensile stress is larger on the leading side of the contact area than that on the trailing side, as shown in Fig. 12(d). This outcome causes the crack to propagate more rapidly on the leading edge side; this result agrees with most of the observations at the monitored site, such as the squats in Figs. 4, 5, 6(c)–(e), 9, 10 and 15. The mechanism of this cracking phenomenon is analogous to that of partial ring/cone crack formation of brittle materials under sphere-sliding contact [29].

In summary, the initiation of the primary crack is caused by tensile stress with mode I fracture at the T1 location, which corresponds to the bottom of the U-shaped crack. The U-shaped crack corresponds to the border of the main contact patch at the depression. This finding was observed at the monitored squats that have crack initiation on the gauge side edge of the depressions, corresponding to the situation in Figs. 12(e) and 13(a).

4.4. Influence of rail inclination on cracking and tertiary cracks

Primary cracks at the squats were typically observed on the gauge-side edge of the black depression. However, cracks could be observed on the field side and at the middle ridge as well as on both the gauge and field sides. These possibilities would happen because the crack initiation location is determined by the position of the main contact area, and the main contact area may vary. The rail inclination plays an important role in determining the position of the main contact area, and the potential positions are shown in Fig. 13.

When the rail inclination is at the nominal value of 1/40, as shown in Fig. 13(a), the presence of the black depression shifts the main contact area to the gauge side. This shift is determined by the contact geometry, namely the profiles of the wheel and the rail, as illustrated in Fig. 12(b) and, especially, Fig. 12(e): the wheel-rail profiles are more conforming to each other on the gauge side than on the field side so that, when there is a depression, the main contact area is usually on the gauge side. As a result, the crack tends to initiate and propagate into a U shape on the gauge side edge of the black depression. This scenario in which the location of the primary crack is on the gauge side (schematically shown in Fig. 12) occurs at most of the monitored squats, such as those squats shown in Figs. 1, 3–10, 15 and 17, the only exception is the case shown in Fig. 14 corresponding to the situation in Fig. 13(c).

Under operating conditions, the effective rail inclination can be different from the nominal state for various reasons, e.g., loose fastenings, which can influence the wheel-rail contact positions and the resulting cracking behavior. For instance, a large increase in the rail inclination causes the wheel and rail to come into the main contact on the field side, and the corresponding primary crack is formed on this side, as illustrated in Fig. 13(c). This scenario was occasionally observed in the continual field monitoring, and an example is shown in Fig. 14. This crack exhibited a U shape with the opening of the U facing toward the field side.

The case between the situations Fig. 13(a) and (c) is a slight increase in the rail inclination that slightly shifts the contact to the field side.

This slight increase, which could render wheel-rail contact simultaneously at both the gauge side and the field side of the black depression, as illustrated in Fig. 13(b), and thus possible almost simultaneous initiation of the primary cracks on both the gauge and field sides, although such a situation has not yet been observed in real life.

For the situation in Fig. 13(a), the main contact area can sink significantly with the development of the primary crack and the growth of the depressed area in both the surface dimension and the depth. The growth of the depressed area increases the excited impact frictional rolling contact forces and contact stress on the main contact area, causing plastic deformation and wear. Therefore, the main contact area may progressively become lower than its less damaged surrounding area. As a result, the main contact shifts to the field side of the depression; the contact position becomes similar to that in Fig. 13(b) and further in Fig. 13(c). This outcome leads to the formation of a tertiary crack on the field side of the depression, as shown in Fig. 15. These tertiary cracks were observed at 24 squats at the monitored site at the time of the fifth and sixth observations. They exhibited a semi-circular crack along the edge of the elliptical edge of the black depressions with the opening of the semi-circular crack facing toward the rail centerline. These cracks could appear before or after the formation of the I-shaped crack described in Section 3.4.2, depending on the rail inclination: the increase in rail inclination could cause the wheel-rail contact at the field side sooner when the main contact area is sinking, which would promote the formation of the subsequent tertiary semi-circular crack on the field side of the depression sooner than the formation of the I-shaped crack.

In summary, there were the following surface cracks observed: primary U-shaped cracks with the opening of the U opposite the black depression (they were usually observed on the gauge side); secondary I-shaped cracks in the middle ridge; and tertiary semi-circular cracks with the opening of the semi-circular cracks facing the black depression.

5. Discussion

5.1. Evolution of the squat geometry and comparison with other types of squats

In this investigation, the squat is induced by the rail surface irregularities of corrugation; in [3], observations of squats were made mainly based on indentation-induced squats. Works in [3,4,14] studied squat growth in the traffic direction and provided evidence that the squats also grew in the opposite-traffic direction. However, this aspect was not explored in detail. The current study proves that the geometry of squats initiated at corrugation grows significantly in the opposite-traffic direction, such as the squats shown in Figs. 4 and 5. The evolution process of squat geometry in the longitudinal direction is schematically illustrated in Fig. 16. In the beginning, a black depression is induced by impact force at corrugation. The black depression grows, and then, a primary U-shaped crack initiates on the edge of the depression. The crack continues to propagate with the U shape in both the traffic and opposite-traffic directions. The shape of the squat evolves following the primary crack in the two directions. When traction force is applied, the crack grows more rapidly in the traffic direction, and length L2 is greater than L1. In the cases of braking, the evolution of the geometry in the traffic direction should have a lower rate, i.e., L2 should be smaller than L1. When the squat grows to a certain size, a peninsula forms. Roughly from this moment on, the development of the squats follows the growth process described in [3], and a middle ridge is produced due to the impact forces caused by the peninsula. As a result, an I-shaped crack is generated at this ridge. The squat then takes on the typical two-lung shape.

Some existing works, e.g., [10,12], have studied crack propagation at squats. These studies concluded that a leading crack was generated first, and then propagated in the opposite-traffic direction to create a trailing crack. The leading crack and trailing crack form the U-shaped cracks at squats. The five-year continual field monitoring in the current study presented a different crack initiation and propagation process, where the cracks initiate at the bottom of U-shaped cracks and grow along the two arms of the U in both the traffic direction and opposite-traffic direction at the same time. The mechanism based on tensile stress reasonably interprets the cracking phenomenon. It is not yet known from the present study if this process and mechanism of the crack initiation and initial growth are applicable to squats from other initiation sources.

Not only corrugation-induced squats but also those squats induced by other sources are developed from initial surface irregularities. These initial irregularities generally do not contain initial cracks. They involve the active type of squat initiation sources, e.g., corrugation and welds, the passive type, e.g., indentation and wheel burns, and the design type, e.g., insulation joints and crossing. The resulting cracks start from the primary virgin cracks. Existing cracks left over by insufficient grinding can develop into squat-like defects and they are sometimes also called squats. These initiation sources are very different, but their resulting squats bear the same characteristic of two-lung shape for mature squats with U, V and Y-shaped macro cracks. The reason for all these disparate initiation sources to converge to the same appearance in the end is their common nature of mechanics. That is, they all excite dynamic contact forces at irregularities, resulting in the two-lung shape, the wavelength of which is determined by that of the dynamic force in relation to the local vehicle-track system. The study regarding to the relation between the wavelength of squat and that of dynamic force has been provided in [3,4] with numerical analysis and field observations. The field observation in the present study again confirms this relation. The characteristic of the wavelength can be used as signature for dynamics-based early detection and track health condition monitoring [16,30]. Timely maintenance based on early detection can not only guarantee operation safety, but also greatly reduce life cycle costs of railway infrastructure [31].

Despite the convergence to the common appearance of mature squats because of the same nature of mechanics, there could be differences in the initiation stages of the squats cracks from the different irregularities. The differences in the process and mechanisms of the initiation of primary cracks and early growth with those of corrugation-induced squats remain to be investigated. Such investigation will facilitate rail material design and selection in relation to loading condition and damage.

5.2. Squat development after rail grinding

During the ten continual observations, rail grinding to a depth of 1.1 mm was performed after the fifth observation. Some of the squat cracks had already propagated more than 1.1 mm into the rails; therefore, the rail grinding did not remove the cracks completely. The remaining cracks grew further and developed into a new squat, as shown in Fig. 17.

6. Conclusions

Five years of continual field monitoring have captured various stages of the life cycle of corrugation-induced squats, from very small black depressions without cracks to mature two-lung-shaped squats typically accompanied by Y-shaped cracks. Based on the observations and analyses of 30 squats, the following conclusions can be drawn.

Short pitch corrugation led to the formation of the squats. The cracks initiated in the surface or at least within the top layer of rail material not deeper than 1.1 mm.

A squat induced by short pitch corrugation started from a small elliptical black depression at the corrugation. The small black depression was formed by the local collapse of a network of microcracks resulting from large plastic deformation and work hardening due to

impact forces.

When the black depression grew to approximately 8 mm in size with the maximum distance of the depression edge on the gauge side edge approximately 6 mm from the rail center, the large tensile stress initiated the first macrocrack at this point of maximum distance from the depression. These 8 mm correspond to the critical size for squat initiation proposed in [13], derived by comparing the maximal von Mises stress with tensile strength, the material being R260Mn. The crack initiation location of 6 mm from the rail center could depend on the contact geometry of wheels and rails, the local track conditions and the material property.

These macrocracks propagated along the border of the main contact area in both the traffic direction and the opposite-traffic direction, forming a U-shaped primary crack in/near the rail surface on the gauge side edge, with the U facing toward the gauge side. The crack initiation point is at the bottom of the U-shaped crack. The crack also propagates into the rail toward the field side at an angle of approximately 20°. The primary crack grew more rapidly in the traffic direction when traction force was applied.

After crack initiation, the squat geometry could not remain fully elliptical. Its gauge side edge became bordered by the U-shaped crack, while the part without cracking remained elliptical, causing the squats at this stage to take on a kidney-like shape. With further growth of the squats along the two arms of the U in the rail surface and the propagation deeper into the rail, the primary cracks gradually formed a peninsula-shaped part that protruded from its depressed surrounding materials. The peninsula-shaped part formed an obstacle to the rolling wheels, causing two impact forces, the first arose when wheels impacted the peninsula-shaped part and the second arose when the wheels feel from the peninsula-shaped part onto the leading edge of the squats. This outcome corresponds to the squat growth process described in [3,4,13,14].

These impact forces, especially the first one, led to a ridge in the middle of the depressed black part of the squats, where a secondary I-shaped crack appeared subsequently. Together with the primary U-shaped crack, it constituted a Y-shaped crack. This Y-shaped cracks divided the black depression into two parts so that the typical two-lung shape of mature squats was formed.

A further tertiary semi-circular crack could occur along the elliptical edge of the depression on the opposite side of the primary U-shaped crack due to sinking of the main contact area.

The change in the rail inclination could shift the wheel-rail impact region so that occasionally the primary U-shaped crack was found on the field side, and the corresponding tertiary semi-circular crack could be found on the gauge side.

In general, the opening of the primary U-shaped crack, regardless of whether on the gauge or field side, is opposite to the black depression. The opening of the tertiary semi-circular cracks faces the black depression.

The findings in the present work contribute to a new understanding of rail RCF. The squat initiation and cracking processes are elaborated and better revealed. The results could help rail engineers perform more effective inspections and plan maintenance more efficiently to reduce costs and improve operation safety. The pin-pointing of the crack initiation location and the identified tensile stress state for crack initiation and propagation should benefit the design and manufacturing of more squat-resistant materials.

References

[1] Clayton P, Allery M. Metallurgical aspects of surface damage problems in rails. Can Metall Q 1982;21:31–46.
[2] Nakamura R, Owaku S, Enomoto N. The rail shelly crack in Japan. Railway Technical Research Institute; 1965. p. 6. [Quarterly reports].
[3] Li Z, Zhao X, Esveld C, Dollevoet R, Molodova M. An investigation into the causes of squats—correlation analysis and numerical modeling. Wear 2008;265:1349–55.
[4] Li Z, Dollevoet R, Molodova M, Zhao X. Squat growth—some observations and the validation of numerical predictions. Wear 2011;271:148–57.
[5] Pal S, Valente C, Daniel W, Farjoo M. Metallurgical and physical understanding of rail squat initiation and propagation. Wear 2012;284–285:30–42.
[6] Pal S, Daniel WJT, Farjoo M. Early stages of rail squat formation and the role of a white etching layer. Int J Fatigue 2013;52:144–56.
[7] Grassie SL, Fletcher DI, Gallardo Hernandez EA, Summers P. Studs: a squat-type defect in rails. Proc Inst Mech Eng, Part F: J Rail Rapid Transit 2011;226:243–56.
[8] Simon S, Saulot A, Dayot C, Quost X, Berthier Y. Tribological characterization of rail squat defects. Wear 2013;297:926–42.
[9] Bogdański S, Lewicki P. 3D model of liquid entrapment mechanism for rolling contact fatigue cracks in rails. Wear 2008;265:1356–62.
[10] Bogdański S. Quasi-static and dynamic liquid solid interaction in 3D squat-type cracks. Wear 2014;314:20–7.
[11] Farjoo M, Pal S, Daniel W, Meehan PA. Stress intensity factors around a 3D squat form crack and prediction of crack growth direction considering water entrapment and elastic foundation. Eng Fract Mech 2012;94:37–55.
[12] Steenbergen M. Squat formation and rolling contact fatigue in curved rail track. Eng Fract Mech 2015;143:80–96.
[13] Li Z, Zhao X, Dollevoet R. An approach to determine a critical size for rolling contact fatigue initiating from rail surface defects. Int J Rail Transp 2017;5:16–37.
[14] Li Z. Squats on railway rails. Wheel-rail interface handbook. Woodhead Publishing; 2009. p. 409–36.
[15] Oregui M, Li S, Núñez A, Li Z, Carroll R, Dollevoet R. Monitoring bolt tightness of rail joints using axle box acceleration measurements. Struct Control Health Monit 2017;24.
[16] Wei Z, Núñez A, Li Z, Dollevoet R. Evaluating degradation at railway crossings using axle box acceleration measurements. Sensors 2017;17:2236.
[17] Grassie SL. Squats and squat-type defects in rails: the understanding to date. Proc Inst Mech Eng, Part F: J Rail Rapid Transit 2011;226:235–42.
[18] Andersson R, Torstensson PT, Kabo E, Larsson F, Ekberg A. Integrated analysis of dynamic vehicle–track interaction and plasticity induced damage in the presence of squat defects. Wear 2016;366–367:139–45.
[19] Hiensch M. Improving track-friendliness of rolling stock. In: Proceedings of the International Heavy Haul Association, Australia; 2015.
[20] Naeimi M, Li Z, Qian Z, Zhou Y, Wu J, Petrov RH, et al. Reconstruction of the rolling contact fatigue cracks in rails using X-ray computed tomography. NDT and E Int 2017;92:199–212.
[21] Morrow J. Cyclic plastic strain energy and fatigue of metals. Internal friction, damping, and cyclic plasticity. ASTM International; 1965.
[22] Tyfour WR, Beynon JH, Kapoor A. Deterioration of rolling contact fatigue life of pearlitic rail steel due to dry-wet rolling-sliding line contact. Wear 1996;197:255–65.
[23] Fine ME. Fatigue resistance of metals. Metall Mater Trans A 1980;11:365–79.
[24] Forsyth P, Ryder D. Some results of the examination of aluminum alloy specimen fracture surfaces. Metallurgia 1961;63:117.
[25] Johnson KL. Contact mechanics. Cambridge: Cambridge University Press; 1987.
[26] Frank F, Lawn BR. On the theory of Hertzian fracture. Proc R Soc Lond: Math Phys Eng Sci: R Soc; 1967. p. 291–306.
[27] Alfredsson B, Dahlberg J, Olsson M. The role of a single surface asperity in rolling contact fatigue. Wear 2008;264:757–62.
[28] Hamilton GM, Goodman LE. The stress field created by a circular sliding contact. J Appl Mech 1966;33:371–6.
[29] Lawn B. Partial cone crack formation in a brittle material loaded with a sliding spherical indenter. Proc R Soc Lond : Math Phys Eng Sci: R Soc; 1967. p. 307–16.
[30] Molodova M, Li Z, Núñez A, Dollevoet R. Automatic detection of squats in railway infrastructure. IEEE Trans Intell Transp 2014;15:1980–90.
[31] Li Z, Molodova M, Zhao X, Dollevoet R. Squat treatment by way of minimum action based on early detection to reduce life cycle costs. In: 2010 Joint rail conference. American Society of Mechanical Engineers; 2010. p. 305–11.